Structural Engineering and Mechanics, Vol. 18, No. 4 (2004) 493-516

DOI: http://dx.doi.org/10.12989/sem.2004.18.4.493

Seismic behavior of high-strength concrete flexural walls with boundary elements

Seung-Hun Kim†

Technical Division, LG Engineering & Construction Corp., Seoul 100-722, Korea

Ae-Bock Lee‡ and Byung-Chan Han‡†

School of Architecture, Chungnam National University, Daejeon 305-764, Korea

Sang-Su Ha‡‡

STRESS, Hanyang University, Seoul 133-791, Korea

Hyun-Do Yun‡‡†

School of Architecture, Chungnam National University, Daejeon 305-764, Korea

(Received December 31, 2002, Accepted June 30, 2004)

Abstract. This paper addresses the behavior and strength of structural walls with a concrete compressive strength exceeding 69 MPa. This information also enhances the current database for improvement of design recommendations. The objectives of this investigation are to study the effect of axial-load ratio on seismic behavior of high-strength concrete flexural walls. An analysis has been carried out in order to assess the contribution of deformation components, i.e., flexural, diagonal shear, and sliding shear on total displacement. The results from the analysis are then utilized to evaluate the prevailing inelastic deformation mode in each of wall. Moment-curvature characteristics, ductility and damage index are quantified and discussed in relation with axial stress levels. Experimental results show that axial-load ratio have a significant effect on the flexural strength, failure mode, deformation characteristics and ductility of high-strength concrete structural walls.

Key words: high-strength concrete; structural walls; ductility; axial loads; strength; earthquake-resistant structures.

---

† Manager
‡ Graduate Student
‡† Lecturer
‡‡ Research Assistant Professor
‡‡† Associate Professor

1. Introduction

In the seismic design of buildings, reinforced concrete structural walls, or shear walls, act as major earthquake resisting members. Structural walls provide an efficient bracing system and offer great potential for lateral load resistance. The properties of these seismic shear walls dominate the response of the buildings, and therefore, it is important to evaluate the seismic response of the walls appropriately. Recently, a high-strength concrete with a compressive strength in range of 60 to 100 MPa has successfully been utilized in columns and core-walls of multi-storey buildings. However, very few experimental works has been reported with reference to the behavior of high-strength concrete structural walls.

Over the past three decades, major advances have been made in the understanding of the behavior of reinforced concrete structural walls, particularly with regard to the role of the variables improving seismic performance (Paulay 1986). However, little experimental work has been done to assess the behavior of reinforced concrete shear walls subjected to high axial load, partly because of the difficulty of applying high axial loads to slender shear walls due to the inherent out-of-plane wall instability problem. Lefas (1988) studied the effect of axial load on strength, stiffness, and deformation characteristics of rectangular walls under a constant axial load and a monotonically increasing horizontal load. As a part a five national research (New-RC) project in Japan, a total of twenty-one high strength, 60 MPa to 120 MPa, concrete shear walls were tested and results were compiled by Kabeyasawa and Hiraishi (1993). The Gupta and Rangan (1998) carried out tests on eight flanged wall specimens subjected to monotonic loading. Zhang and Wang (2000) investigated the influence of axial-load ratio and shear compression ratio on the behavior of rectangular shear walls. While little research has been carried out on the framed walls under high gravity load and seismic action, high-strength concrete framed walls are becoming more frequently used as the lateral resisting elements in wide-bay high-rise buildings. This investigation is an exploratory phase of an experimental program of high-strength concrete framed walls subject to the combined action of constant high axial load and reversed cyclic horizontal loading.

2. Experimental program

The experiment included testing of three one-third scale framed flexural walls with height-to-width ratio (h_w/l_w) of 1.80. Such walls with a barbell shaped cross section are typical in the lower stories of a prototype 60-story office building located in a moderate seismic zone.

The scope of the experiment was limited to tests on isolated wall specimens. The test specimens were subjected to constant axial compressive force and reversed cyclic horizontal loading. All the specimens were designed based on the philosophy that the lateral load capacity was controlled by flexure and therefore, the undesirable premature shear failure during the experiment would be prevented. The overall dimensions of the test specimens were kept constant.

Three isolated flexural walls, as shown in Fig. 1, were constructed and tested in this investigation. The dimensions of the specimens correspond to one third the dimensions of the prototype. To scale down the prototype structure to the specimens, two independent scale factors were chosen for stress and length, respectively; all remaining scale factors were either equal to unity or were functions of two factors. Each wall was tested under combined action of constant axial load and horizontal load reversals. All three wall specimens, HW1 to HW3, had boundary elements. Boundary element transverse reinforcement, 6 mm diameter hoops spaced at about 40 mm, was selected in a way such that adequate confinement to core concrete would be provided, and longitudinal reinforcement

Table 1 Details of test specimens

Wall specimen	Axial-load ratio	Storey beam reinforcement ratio (%)	Wall			Boundary element		
			W × H × T (m × m × mm)	ρ_v (%)	ρ_h (%)	B × D (mm × mm)	ρ_f (%)	ρ_s (%)
HW1	0.24	1.11	1.2 × 2.0 × 85	0.55	0.55	180 × 180	1.75	0.78
HW2	0.12	1.11	1.2 × 2.0 × 85	0.55	0.55	180 × 180	1.75	0.78
HW3	0.00	1.11	1.2 × 2.0 × 85	0.55	0.55	180 × 180	1.75	0.78

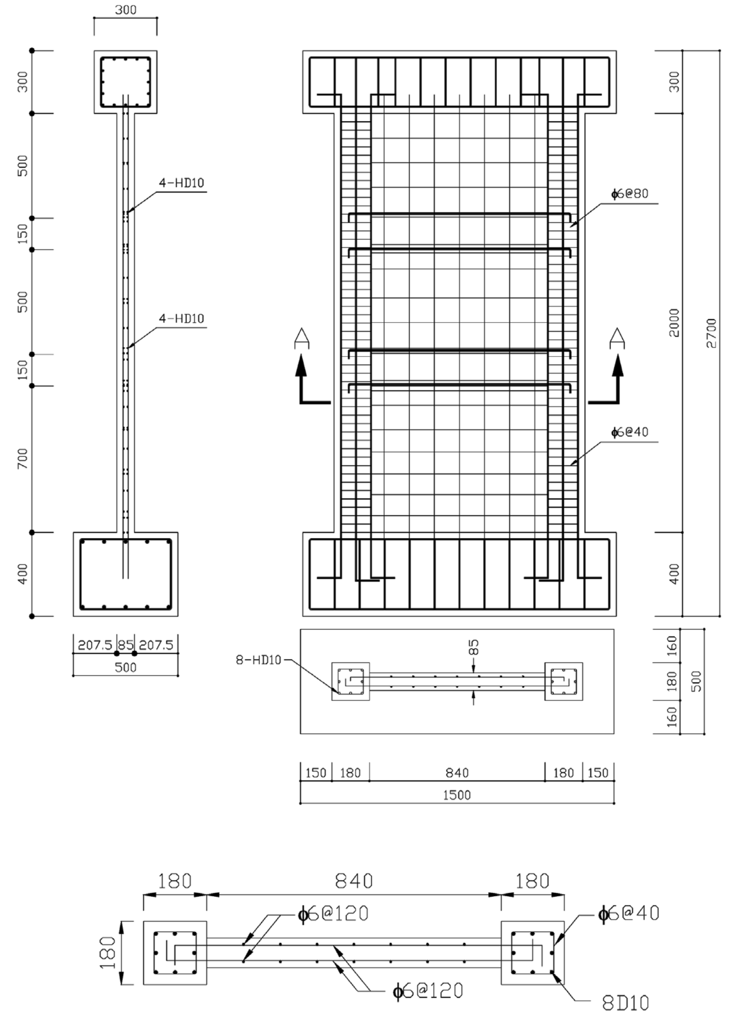

Section A - A

Fig. 1 Geometry and reinforcement details(section A-A) of wall specimens (unit : mm) buckling in the post-yielding stage would also be prevented. The geometry, dimensions, amount and arrangement of boundary elements of walls were identical for all three specimens. The main flexural reinforcement of each boundary element consisted of eight 10 mm diameter high-tensile deformed steel bar arranged in a rectangular manner.

All the specimens had the same geometry and were monolithically connected to the top and foundation beam. A heavily reinforced top beam (1.50 m long × 300 mm deep × 300 mm wide) functioned as both a uniform load transfer through which axial and horizontal loads were applied to the walls and as a cage for anchorage of the vertical bars. The foundation beam (1.50 m long × 400 mm deep × 500 mm wide) was utilized to clamp the specimens to the laboratory floor, simulating a rigid foundation. A summary of the experimental program is presented in Table 1. The overall geometry and dimensions of the wall specimens and reinforcement details are shown in Fig. 1.

All the specimens were designed using 0.55% horizontal and 0.55% vertical web reinforcement ratios. Vertical reinforcement consisted of 7 pairs of 6 mm diameter high-tensile round steel bar, uniformly placed in two layers. Uniformly distributed horizontal web steel consisted of two layers of 6 mm diameter high-tensile round steel bar. The bars were spaced at 120 mm along the full height of the wall. The horizontal bars were anchored into the core of each boundary element using 90-degree hooks.

All reinforcing bars were provided with adequate anchorage lengths at their ends. This was achieved by providing cogs at the ends of the bars. All closed ties were terminated with 135-degree hooks. In all specimens, the clear concrete cover to reinforcement was 20 mm. Additional horizontal reinforcement, four 10 mm diameter deformed bars, was arranged at each floor slab level.

2.1 Material properties

Commercial ready-mixed concrete with replacement of 7.8% (by weight) cement by silica fume was used and was made using a selected ASTM Type I Portland cement. A high-range water reducer (superplasticizer) and water-reducing retarder were added to the mix to improve workability. The specified 28-day compressive strength of the mix was 68.7 MPa. The maximum size of aggregate was 15 mm in order to ensure good compaction of concrete in the test specimen. The slump of the concrete was 150 mm. For each batch, 100 × 200 mm cylinders were made to measure the compressive strength and the splitting tensile strength of concrete. The measured concrete strength and elastic modulus were tested by the ASTM standard test method. The compressive strength and the splitting tensile strength on the day of the wall test are given in Table 2.

The reinforcing steel for all the walls was obtained from one batch of steel for each bar diameter. Three samples were taken and tested from each diameter of reinforcing used. Tension tests were conducted on full-size bar samples in accordance with ASTM A370 to determine yield strength, ultimate strength, and total elongation. Physical properties of reinforcing steel are given in Table 3.

Table 2 Average concrete compressive strengths

Compressive strength (MPa)				Slump (mm)	Elastic modulus (MPa)	Poisson's ratio
5-day	7-day	28-day	90-day*			
42	63	65	69	150	33,150	0.11

*At the time of testing

Table 3 Properties of reinforcement bars

Type	Yield strength f_{sy}, (MPa)	Ultimate strength f_{su}, (MPa)
10 mm diameter deformed bar	413.9	664.0
6 mm diameter round bar	571.8	636.5

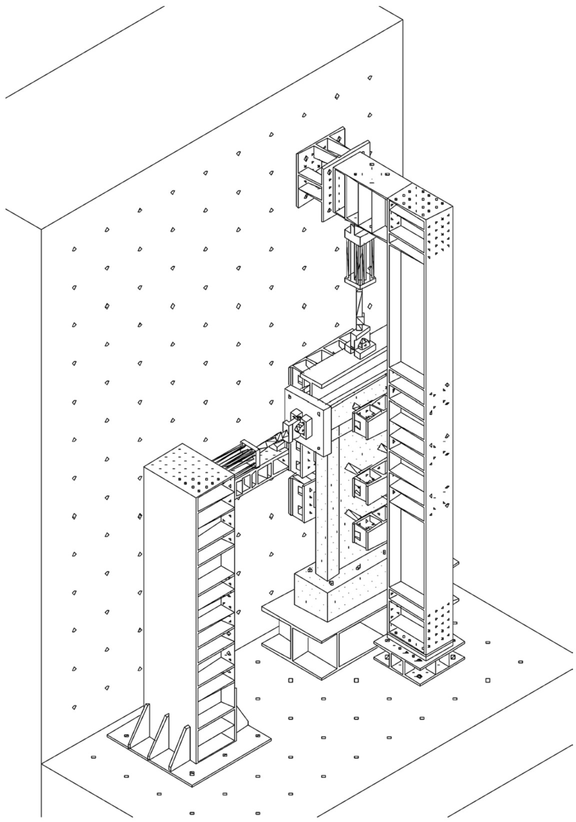

Fig. 2 Test setup

The test wall specimens were monolithically connected to foundation beams and cast horizontally in timber molds.

2.2 Testing apparatus

The testing apparatus is shown in Fig. 2. The wall footing is rigidly connected to the strong floor using eight 32 mm diameter high-tension bolts. A 980 kN MTS hydraulic actuator attached to the reaction frame was used to apply a horizontal force to the load transfer assembly mounted on the top of the wall. To ensure out of plane stability and represent the diaphragm effect of a floor slab, the wall is laterally guided by low friction sliding ball bearings at the levels of the first and second floor. Axial load was provided with a 980 kN MTS hydraulic actuator on the top of the load transfer assembly and maintained concentric to the test wall at all stages of loading.

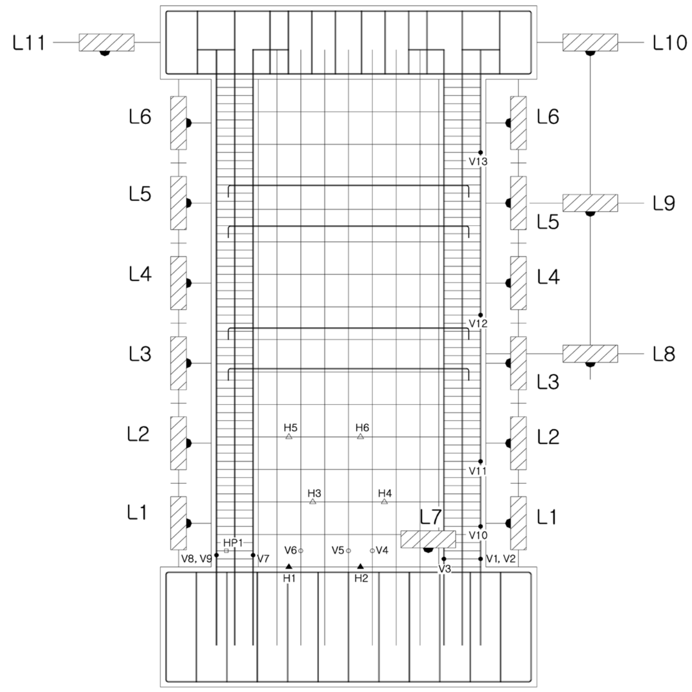

Fig. 3 Instrumentation arrangement

2.3 Instrumentation and data acquisition

The data acquisition system consisted of thirty-six internal control and recording channels. Instrumentation was provided to measure loads, displacement, and strains at critical locations. Lateral and axial load were measured using load cells capable of maintaining linearity up to 980 kN. The load cells were calibrated before and after each test in a test machine. As shown in Fig. 3, the displacements of each specimen were measured using Linear Variable Differential Transducers (LVDTs). Two LVDTs were installed at the top of the specimen to monitor the top displacement. The horizontal displacement profile of each specimen was measured using LVDT at each storey level (at three locations over the wall height). One LVDT was installed at a distance of 100 mm from the wall base to measure the sliding of the base. Twelve LVDTs were installed close to the boundary elements to measure the curvatures along the height of walls to obtain the flexural deflection. Steel strain gages were also provided on numerous hoops and cross ties within the boundary elements and on horizontal and vertical reinforcement within the web. The foregoing system of measurements made it possible to estimate the flexural, shear, and sliding components of the wall deformation.

2.4 Testing procedure

A constant axial load was first applied through a spread beam at the centers of the boundary elements of walls. HW1 to HW3 were subjected to three levels of axial-load ratio corresponded to 0.24, 0.12, and 0.00 of the uniaxial compressive strength of the boundary elements cross-section that is equal to $0.97f_cA_{cg}$. These levels of axial load might be considered representative of the amount at the base of a single storey, medium-rise, and high-rise building, respectively. During each test, the displacement at the top of the wall was controlled.

A reverse cyclic loading was applied slowly to the top of the specimens. Initially, the test specimen was exercised by applying 49 kN horizontal load in order to ensure that all systems were working. The initial load was then released and zero reading was taken. The walls were cycled three times at each of the incrementally increasing deflection level until failure. The deflection increments were based on yield deflection. The yield deflection was determined by drawing a straight line from the origin through the first yield load and its intersection with a horizontal line drawn at calculated ultimate load level. The first yield load was obtained experimentally when the strain gages on the extreme tension reinforcement at the boundary elements yielded.

3. Experimental results

3.1 Cracking process and failure mode

Flexural cracks initially appeared at the base of the boundary elements in the tensile zone during the first elastic loading, and the cracks propagated from the wall boundary elements toward the center and from the bottom upwards. These cracks were initially horizontal and confined within the length of the boundary elements, but as the loading increased, they became slightly inclined downwards and extended into the web (see Fig. 4). Eventually, these cracks formed a diagonal cracking pattern in the web. The inclination increased along the wall height. At the boundary elements, the density of the cracks increased, while in the web the number of main cracks was limited to about four or five on each side. In the lower part of the wall, flexural cracks originating from one edge were intersected by inclined shear or flexural-shear cracks originating from the opposite edge, resulting in a characteristic criss-cross pattern. With cycling to increased deformations, the rhomboidal pieces of concrete between the intersecting cracks gradually deteriorated and spalling of cover concrete occurred. The spalling zone extended further upwards in the case of specimen HW3, which was subjected to horizontal load without axial force (see Fig. 5(c)).

Significant loss of strength, leading to failure, was observed when concrete started to deteriorate in the most heavily stressed parts of the boundary elements. The web, hoops, and horizontal bars

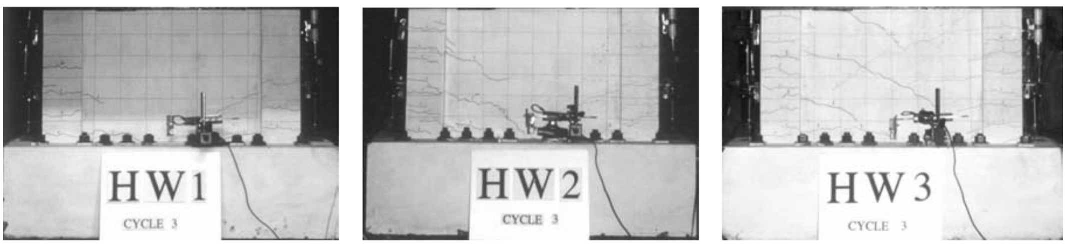

(a) HW1 (b) HW2 (c) HW3

Fig. 4 Cracking pattern at the yielding stage

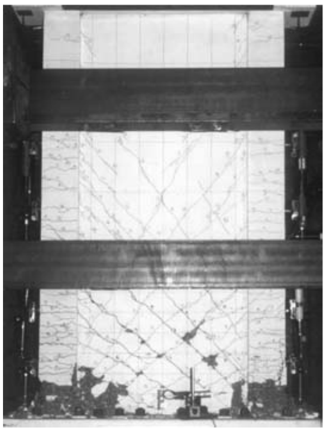
(a) HW1

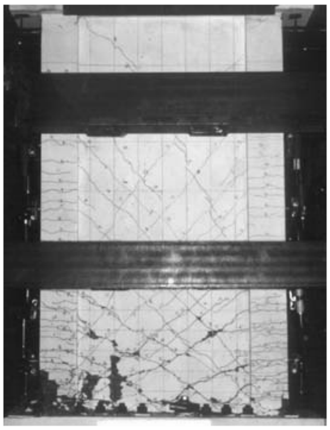
(b) HW2

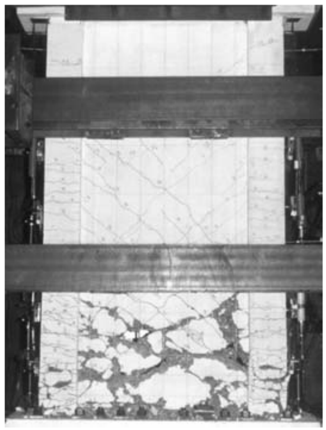
(c) HW3

Fig. 5 Failure modes

began to lose support and move away from each other as buckling and kinking of the longitudinal bars occurred. The effects of the axial stress ratio on the cracking pattern and failure mode of the specimens can be seen in Fig. 5. Because wall behavior was controlled by flexure, the cracking process was similar for all specimens (see Fig. 4).

Observed cracking patterns at yielding and failure are shown in Figs. 4 and 5. High axial stress ratios restrained the development of major inclined cracks in the web. This is because increased axial force will reduce the principal tensile stress in the web portion of the wall. The presence of higher levels of constant axial force led to even less extensive crack formation. Fewer flexural cracks were formed at the tensile edge of the wall and diagonal cracking covered less of the web of the wall. Nevertheless, higher axial force levels only managed to delay but not prevent the extension of the inclined crack within the lower compressive edge of the boundary elements.

3.2 Load-displacement response

Base shear force versus top displacement hysteresis loops for all specimens are shown in Fig. 6. In the figure, the well-known characteristics of reinforced concrete members subjected to cyclic loading, such as unloading and reloading stiffness reduction as the cyclic displacement amplitude increases and pinching of hysteresis loops can be clearly seen. Some ductility was observed for specimens subjected to large axial forces (see Fig. 6(a) through (c)). As axial force was increased, load-displacement curves showed an S shape hysteresis loop with small residual displacements.

The strength of all specimens except HW3 increased due to the presence of the compression axial force, but ductility was slightly inferior to that of HW3. Significant strength degradation occurred at a displacement of 52 mm (2.65% drift) following extensive concrete crushing and reinforcement buckling at the boundary elements; further cycling led to eventual fracture of some buckled bars. Hence, inelastic performance of high-strength concrete structural walls represented stable behavior in flexural yielding and maintaining horizontal load-carrying capacity.

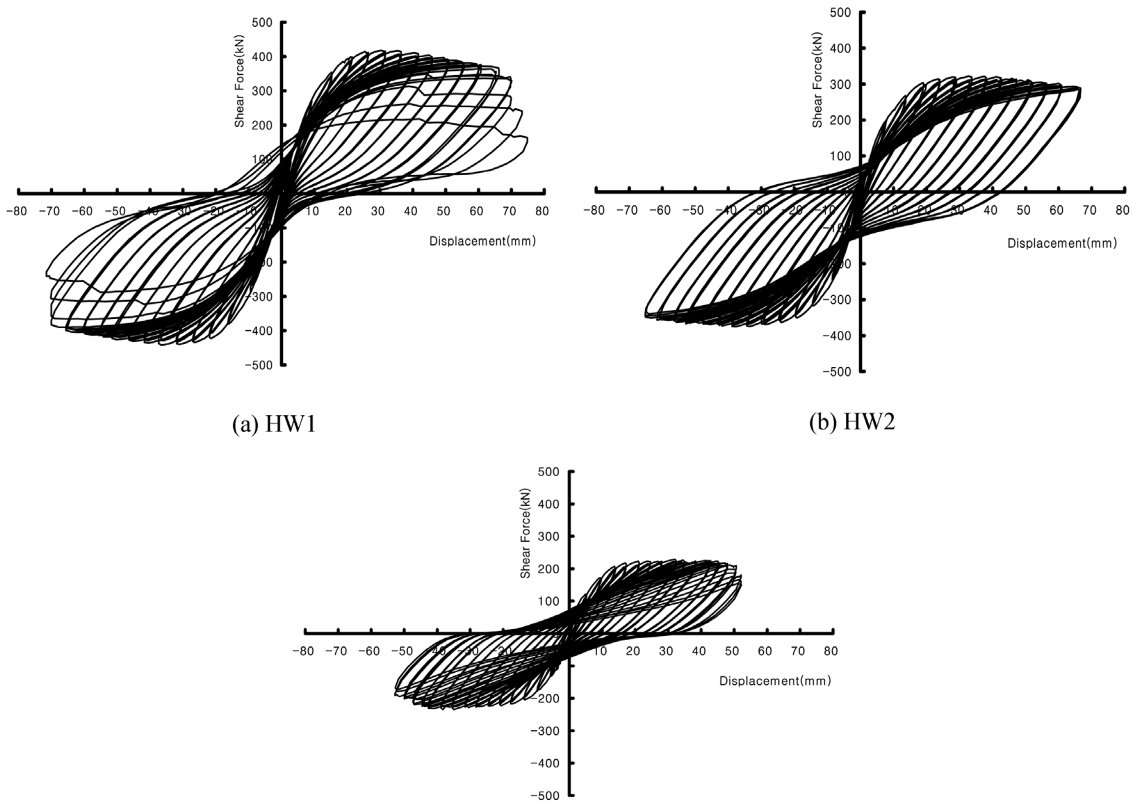

(a) HW1 (b) HW2

(c) HW3

Fig. 6 Horizontal load versus top horizontal displacement

3.3 Strength, stiffness and energy dissipation characteristics

Predicted results of ACI Building Code (2002) and Architectural Institution of Japan (AIJ) Guideline (1994) are summarized in Table 4 and compared with the experimental values. Predicted flexural strength of the specimen HW3, which was not subjected to axial force, was almost the same as the observed load-carrying capacity of specimen. For the specimens HW1 and HW2 with axial stress ratio of 0.24 and 0.12 (on the boundary elements) respectively, the measured strengths of these specimens were larger than their predicted strengths by approximately 13%. This can be attributed to the enhanced concrete strength due to confinement from surrounding concrete. The ACI 318-02 and AIJ Guideline seem to be slightly conservative in this respect.

The reduction of strength and stiffness of reinforced concrete, especially high-strength concrete, members subjected to cyclic loading are significant for structures in seismic areas. Therefore, seismic resistant members with significant degradation of strength and stiffness due to the imposition of severe cyclic loading must be avoided in seismic design. Fig. 6 indicates that the horizontal load-carrying capacity of a wall is dependent on the level of axial force. Table 4 also indicates that the strengths of the walls with axial stress ratio of 0.12 and 0.24 was greater than that of the wall subjected to only horizontal load by about 60.2% and 88.8%, respectively. The

Table 4 Correlation of test and predicted strengths (Unit : kN)

Specimen	ACI 318-02 (2002)						AIJ Guideline (1994)			Experimental results
	Flexural strength		Shear strength				Flexural strength		Shear strength	
	V_y	V_u	V_s	$V_c + V_s$	V_n	Upper limit	V_y	V_u	V_q	
HW1	332.7	387.0	256.0	537.5	449.6	677.2	316.1	383.7	546.7	442.0
HW2	272.4	331.5	256.0	475.9	449.6	677.2	355.7	293.5	513.3	375.0
HW3	173.3	241.2	256.0	395.4	449.6	677.2	103.7	161.5	469.6	234.1

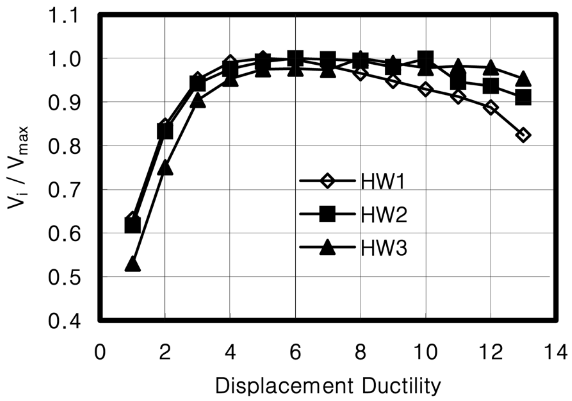

Fig. 7 Degradation of strength (V_i/V_{max})

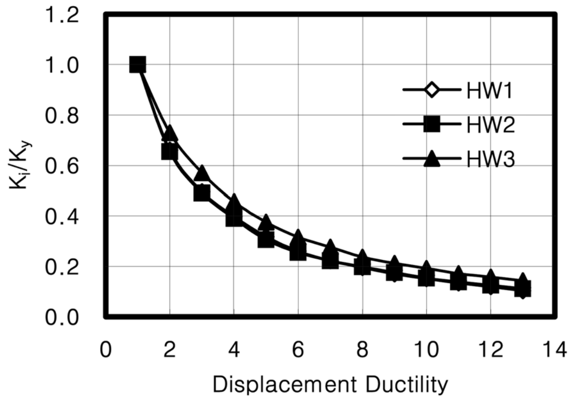

Fig. 8 Degradation of stiffness (k_i/k_y)

maximum shear load for each displacement step, V_i, is plotted as a fraction of the maximum shear strength, V_{max}. The data are plotted versus the displacement ductility ratio (δ_i/δ_y) shown in Fig. 7 for all walls.

The stiffness characteristics of high-strength concrete flexural walls, which are a function of the slopes of the load-deformation curves, were influenced considerably by the effects of the level of axial force. Stiffness characteristics of structural walls were dominated by a severe loss of stiffness during and after yield. A principal cause for the loss of stiffness in walls was the diagonal shear crack and crushing of wall web concrete. All of the specimens showed an increase in secant stiffness values as the applied level of constant vertical stress increased. In early stages, the secant stiffness of HW1 was higher than that for HW2 and HW3. However, with increasing loading cycles, the variation of secant stiffness for HW3 was more stable than that of HW1 and HW2. It can be concluded that axial force has a detrimental effect on stiffness variation in the post-yielding stage of flexural wall deformation. Stiffness decay as noted by the relation between the ratio k_i/k_y and displacement ductility is shown in Fig. 8, where k_i is equal to the secant stiffness values corresponding to the first half-cycle in each stage.

Energy dissipation under cyclic loading was defined as the area enclosed by the base shear force versus top displacement hysteretic loops shown in Fig. 5. The amount of energy dissipated prior to

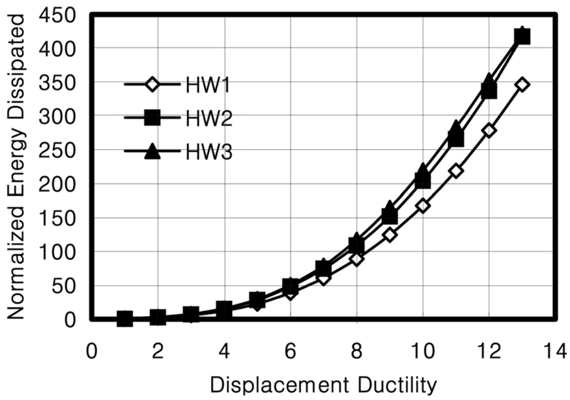

Fig. 9 Normalized energy dissipated

first significant cracking of the wall was relatively small, but increased greatly once this level was exceeded. It is obvious that energy dissipation capacity rose with the increase of axial stress ratio. The relationship between normalized energy dissipated and displacement ductility is summarized in Fig. 9. The normalized energy dissipated was defined as the energy dissipated in half hysteresis loop corresponding to positive load direction divided by $0.5V_y\delta_y$, where V_y and δ_y are the yielding load and yielding displacement, respectively. As noted by comparing curves for specimens HW1 and HW3, high axial force had a detrimental effect on energy dissipation behavior.

Total energy applied to the wall during virgin loading can be separated into three components, namely, the recoverable energy, damping energy, and the damage energy. The energy dissipated by a wall is the sum of the damage energy and the damping energy. Another way of presenting the energy dissipated per cycle during a cyclic loading test is by using the concept of equivalent viscous damping. This term has been used by investigators to correlate hysteretic energy dissipation to the standard concept of structural damping used for linear systems. Generally, measurements of dynamic response of actual structures in the elastic range close to the yield strength indicate that equivalent viscous damping levels of 5% to 7% for reinforced concrete are appropriate (Paulay and Priestley 1992). In the elastic range close to yield strength, the equivalent viscous damping level of high-strength concrete flexural walls tested was approximately 5%.

3.4 Components of displacement

An attempt has been made to assess the contribution of each deformation component on total displacement of the wall specimens. The deformation components include flexural, shear in the web, and the horizontal sliding shear deformation at the base. The sliding shear deformation component was measured with LVDTs attached between the footing and the wall panel. The flexural component was calculated as the sum of the average measured layer curvature multiplied by each layer height. The shear component was then evaluated by the measured top displacement subtracted by the above two components. Fig. 10 displays a typical example of hysteresis loops for HW1 and HW3 specimens with and without axial force, respectively.

The contribution of each deformation mode to the total displacement of wall specimens is shown in Fig. 11 for various ductility levels. It is clear from the figure that the relative contribution of each

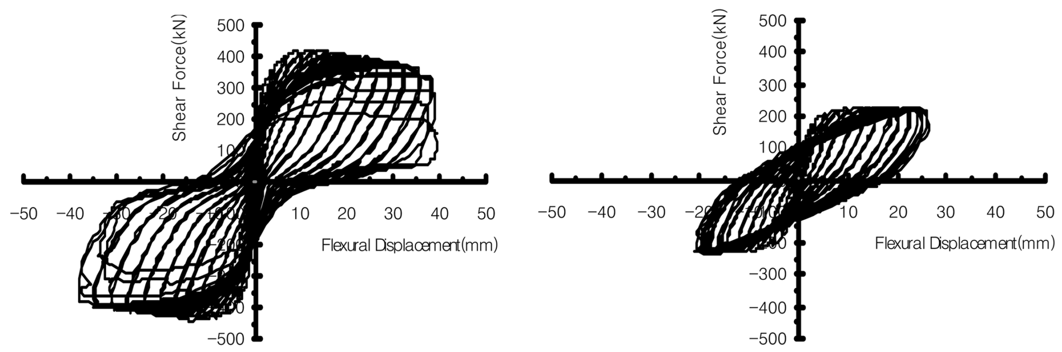

HW1 Specimen HW3 Specimen

(a) Shear force versus flexural displacement

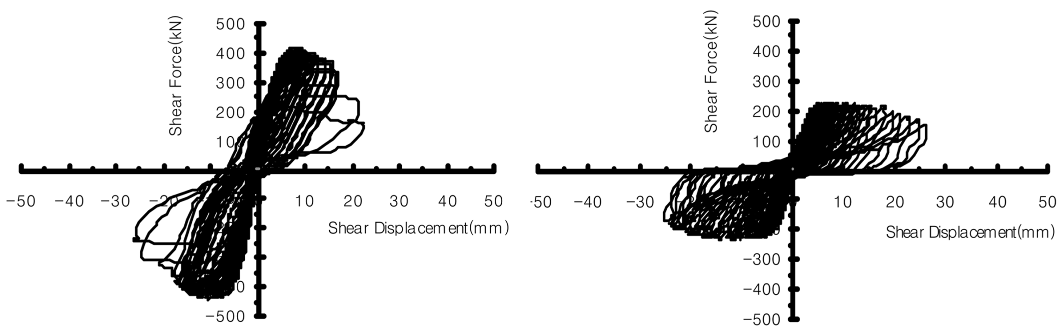

HW1 Specimen HW3 Specimen

(b) Shear force versus shear displacement

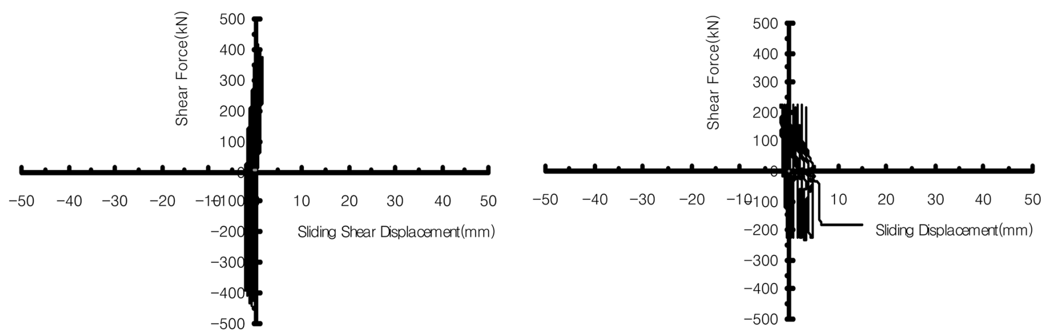

HW1 Specimen HW3 Specimen

(c) Shear force versus sliding displacement

Fig. 10 Hysteresis loops for HW1 and HW3 specimens

component is significantly varying with the ductility level. Initially, shear deformation dominated the response. However, after yielding, flexure deformation governed the response, being a major contributor to the total displacement. For the high axial-load ratio wall specimen HW1, shear

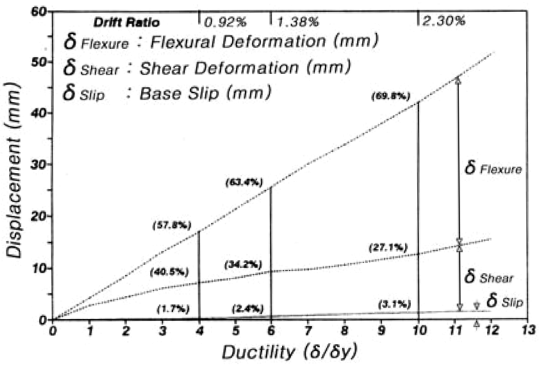

(a) HW1

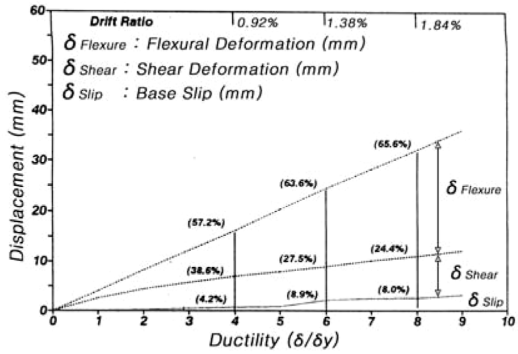

(b) HW2

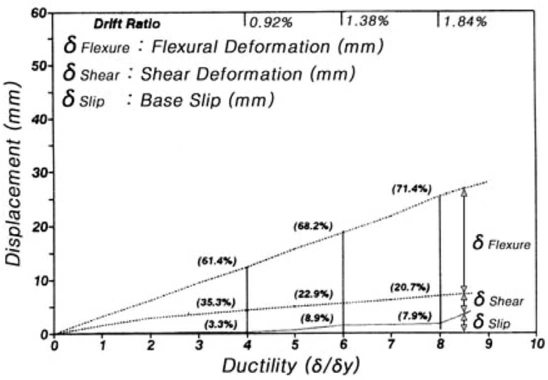

(c) HW3

Fig. 11 Displacement components

deformation reached up to 64% of the total displacement at yielding. However, as the ductility is increased (2 or more), flexural deformation is more pronounced, being approximately 55% of the total displacement. It is noted that the sliding shear deformation component was minor, being 0.4% and 3.1% of the total displacement at yielding and at close to failure, respectively. Whereas the deformation modes of the HW2 specimen were similar to those of HW1 shown in Fig. 11(a), the contribution of sliding shear deformation was considerable (approximately 19% of the total displacement at ductility of 9) for the HW3 specimen without axial force.

For most of walls, the contribution of shear deformation was significantly lower than that of flexural deformation. As expected, compressive axial played a significant role on the reduction of base sliding and shear deformation, respectively.

3.5 Curvature distribution

Twelve LVDTs were mounted along the centerline of each boundary element on opposite faces (tension and compression), as shown in Fig. 3. The average curvature of specific sections of the wall was then obtained from the readings of each LVDT.

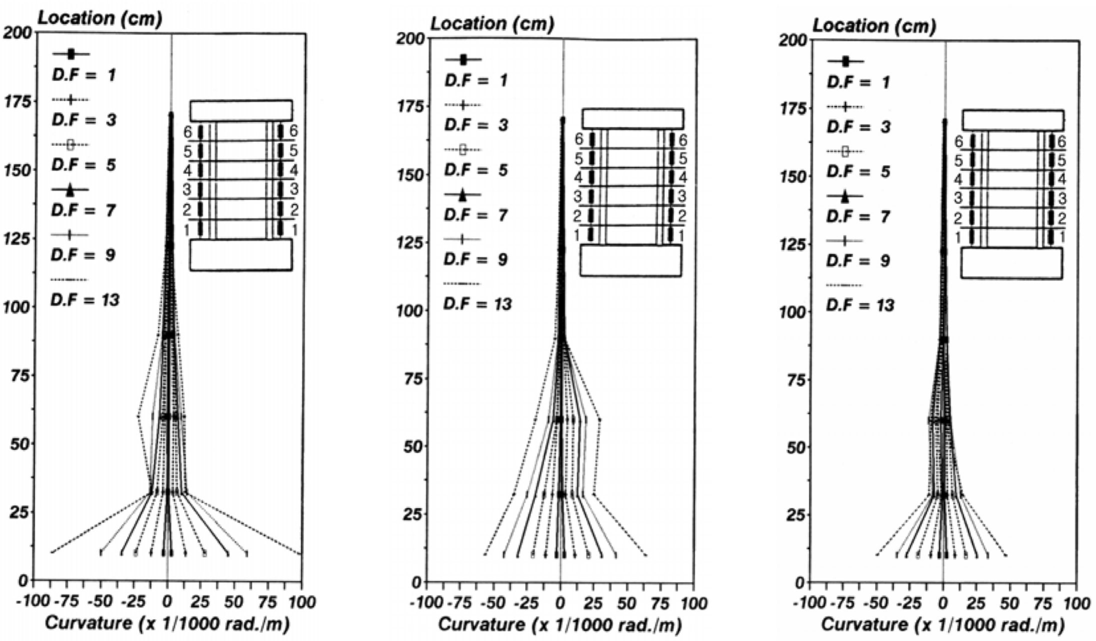

(a) HW1 (b) HW2 (c) HW3

Fig. 12 Curvature distribution (1 cm = 10 mm)

The vertical distributions of curvature along the wall height with different axial-force ratios are shown in Fig. 12(a) through (c). At the location of each of the LVDTs (L1 - L6 as shown in Fig. 3), the average curvature was calculated, and the corresponding points were connected by straight lines to show an approximate variation of the curvature along the wall height. The reduction in average curvature from L4 to L6 is due to the fact that additional horizontal bars at the second floor level prevented diagonal cracks from extending. By comparing Figs. 12(a) and (c), one can see the concentration of plastic rotation at the base of the wall as the axial-force ratio was increased. The influence of axial force was to propagate the plastic rotation to the upper part of the wall.

3.6 Moment curvature

Moment-curvature relationships for specimens, HW1, HW2, and HW3 were constructed in terms of a monotonically increasing curvature. Following assumptions have been made in the moment-curvature analysis: 1) the plane section before bending remains plane after bending, 2) stress-strain relationships of the reinforcement in both tension and compression, as shown in Fig. 13(a), 3) stress-strain relationship of a high-strength concrete in compression, taking into account the confinement effect (Razvi and Saatcioglu 1999) as shown in Fig. 13(b). After tensile cracking, the tensile capacity of a concrete depends primarily on the reinforcing steel and thus the tensile-stiffening effect is also taken into account (Gupta and Maestrini 1990).

Fig. 14 shows the experimental and analytical moment-curvature relationships for three of the high-strength concrete structural walls tested. Whereas the thin solid lines indicate cyclic

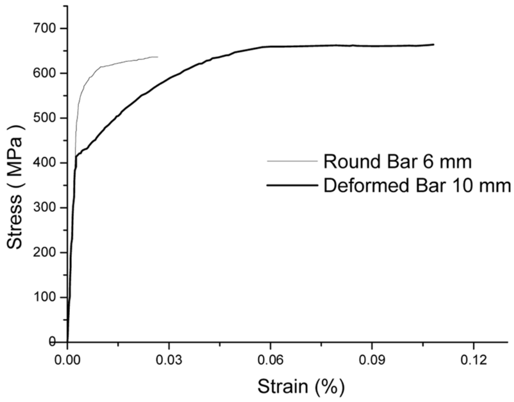

(a) Steel stress-strain relationship

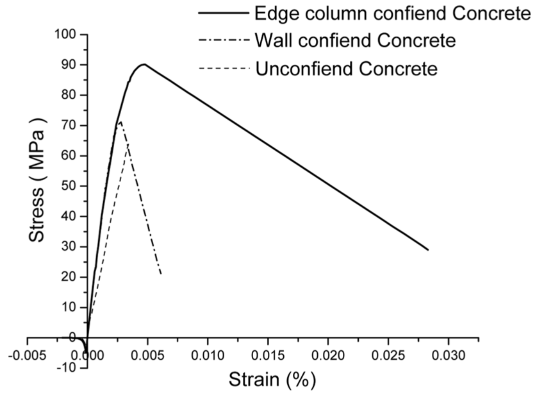

(b) Concrete stress-strain relationship

Fig. 13 Material stress-strain relationship

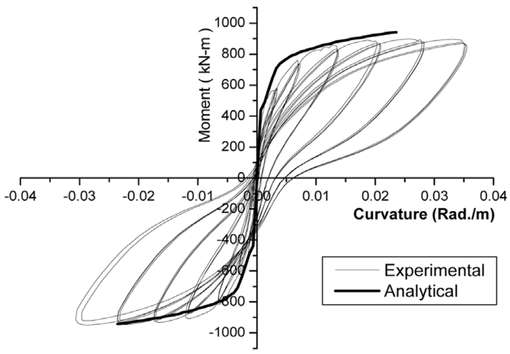

(a) HW1

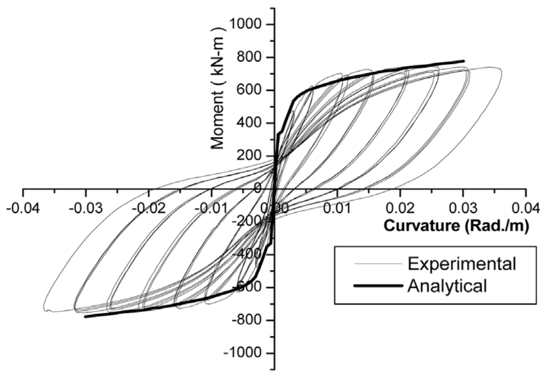

(b) HW2

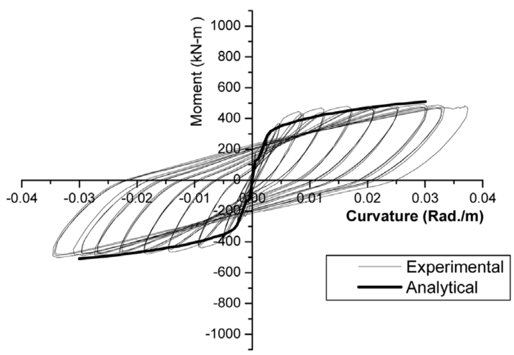

(c) HW3

Fig. 14 Moment versus curvature at wall base experimental results, the thick solid lines describe the monotonic envelopes generated by the average strain model. The experimental and analytical moment-curvature relationships exhibit a well-defined yield point followed by a nearly horizontal yield plateau. For Specimen HW3 with a horizontal load only, the envelope for the experimental moment-curvature curve is slightly greater than the analytical curve. However, for specimens HW1 and HW2 having a relatively higher axial-load ratio than HW3, good correlation has been achieved between the experimental and analytical moment-curvature curves. Both yield moment and curvature have been predicted within a reasonable accuracy. The initial experimental stiffness shows also a good agreement with that predicted by the analytical moment-curvature model. This can be attributed to the fact that the analytical model takes into account the tension stiffening effect in a cracked concrete. In general, the present study demonstrates that the analytical moment-curvature model is capable of predicting the response of high-strength confined concrete. It is to be noted that shear does not seem to have a significant effect on the moment-curvature response.

3.7 Ductility

The term ductility defines the ability of a structure and selected structural components to deform beyond elastic limits without excessive strength or stiffness degradation. The most convenient quantity to evaluate either the ductility imposed on a structure by an earthquake or the structure's capacity to develop ductility is displacement ductility as Eq. (1).

$$\mu_\delta = \frac{\delta_u}{\delta_y} \tag{1}$$

Where, δ_y is top displacement at yielding (as the point of initiation of a pronounced non-linearity of the horizontal force versus the horizontal displacement curves); δ_u is the displacement at the point when the shear resistance level decayed to 85% of the observed maximum strength. The δ_u, displacement at 85% of the maximum horizontal force with the descending branch of the envelope of the hysteresis loop are taken as these at failure. This definition is in agreement with the 15% force response degradation of reinforced concrete elements acceptable by Eurocode 8 (1994).

Table 5 and Fig. 15(a) show the effect of the two parameters investigated, namely the axial-load and the horizontal web reinforcement ratio, on ductility of high-strength concrete structural walls. In fact, by comparing the displacement ductility values for HW1, HW2, and HW3, which had the same horizontal reinforcement ratio but a different normalized axial-load ratio (equal to 0.24, 0.12, and 0.00 on the boundary elements respectively), one may observe that for this axial load increase, the ductility decreased from 13.69 to 11.93 (13% reduction).

Table 5 Measured displacement response, ductility factor, and damage index

Wall specimen	Displacement (mm)		Displacement ductility (μ_δ)	Normalized energy index (E_n)	Work index (W_i)
	δ_y	δ_u			
HW1	4.30	51.30	11.93	253.0	1538.20
HW2	4.08	52.47	12.86	346.6	2413.27
HW3	3.24	44.36	13.69	417.1	2793.80

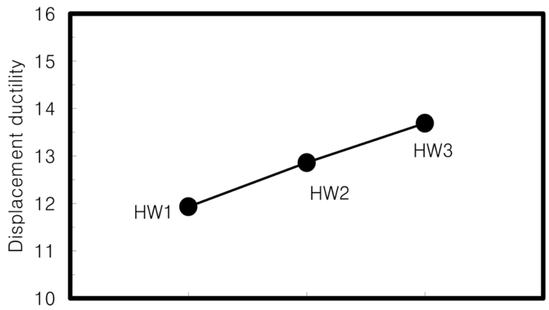

(a) Ductility

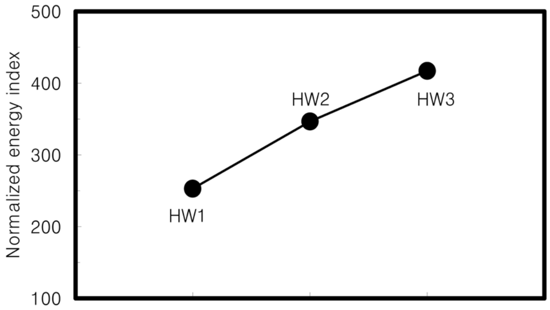

(b) Damage index

Fig. 15 Damage index of walls

3.8 Damage indexes

Many authors have established a set of damage indexes to ascertain the residual capacity of structures. A wide array of parameters may be used, such as number of cycles, stiffness, and ductility. When reverse loads are applied, however, the importance of energy dissipation is readily apparent. The energy indicator proposed by Darwin and Nmai (1986) provides an assessment of the dissipative capacity compared with the elastic energy injected at peak load. This measurement has been related to the hysteretic area of cycle i, E_i normalized to the elastic energy $F_{\max}\delta_{F\max}$. The iteration on all cycles yields the total normalized cyclic energy, as follows

$$E_n = \frac{\sum E_i}{F_{\max}\delta_{F\max}} \tag{2}$$

This indicator has been modified by Ehsani and Wright (1990) through introducing a damage index combining the cyclic dissipated energy, the stiffness degradation and the deformation capacity

$$W_i = \frac{\sum E_i}{F_{\max}\delta_{F\max}}\left(\frac{k_i}{k_y}\right)\left(\frac{\delta_i}{\delta_y}\right)^2 \tag{3}$$

Where, $F_{\max}$ is peak load; $\delta_{F\max}$ and δ_i are deflection at the peak and maximal deflection of cycle i, respectively; E_i is dissipated energy calculated from the area of cycle i; and k_y and k_i are secant stiffness at the yielding and in cycle i, respectively.

To evaluate the effect of axial load in boundary element and transverse web reinforcement on the seismic resistance of high-strength concrete structural walls, two comparisons in damage index, E_n and W_i, were made between specimens and reported in Table 5. As axial stress in boundary elements increases, damage index reduced significantly. Therefore, while axial stress increases the horizontal load carrying capacity and secant stiffness, it improves the seismic resistance of high-strength reinforced concrete structural walls inefficiently.

4. Ductility and detailings of wall boundaries

Displacement-based design procedure, proposed by Wallace (1994), of slender reinforced concrete walls provides a versatile and flexible design format for evaluating detailing requirements at wall boundaries. The procedure involves comparing the strain capacity of the wall with the estimated strain imposed on the wall as a result of a design earthquake. In general, the strain capacity of a wall can be increased by providing additional transverse boundary reinforcement. Thus, confinement in the boundary element is provided based on the deformation and strain demand rather than on an arbitrary nominal value.

The procedure presented herein to determine the need for boundary concrete confinement for high strength concrete framed walls is based on analytical methods. Available experimental data for high strength concrete shear walls with boundary elements are reviewed in the following sections to evaluate the validity of portions of the analytical studies.

The deformation imposed on individual walls as a result of the global building deformations can be evaluated using well-established procedures to account for the distribution of elastic and inelastic deformations over the wall height. Based on the wall system subjected to a linearly increasing distribution of lateral forces over the wall height shown in Fig. 16, the displacement at the top of the wall can be computed as

$$\delta_u = \delta_y + \theta_p h_w = \frac{1}{3}\phi_y h_w^2 + \frac{1}{2}(\phi_u - \phi_y) h_w l_w \tag{4}$$

where δ_y is displacement resulting from elastic deformations; $\theta_p h_w$ is displacement resulting from inelastic deformations; l_w is wall height; h_w is wall length; ϕ_y is yield curvature (curvature at first yield of the wall boundary reinforcement); ϕ_u is ultimate curvature; and θ_p is plastic rotation, respectively. Based on this relation and assumptions for yield curvature, $0.0025/l_w$ and plastic hinge length, $0.5l_w$, the deformations imposed on a wall can be derived in terms of the ultimate curvature times the wall length (Wallace and Moehle 1992). With this approximation, the curvature ϕ_u

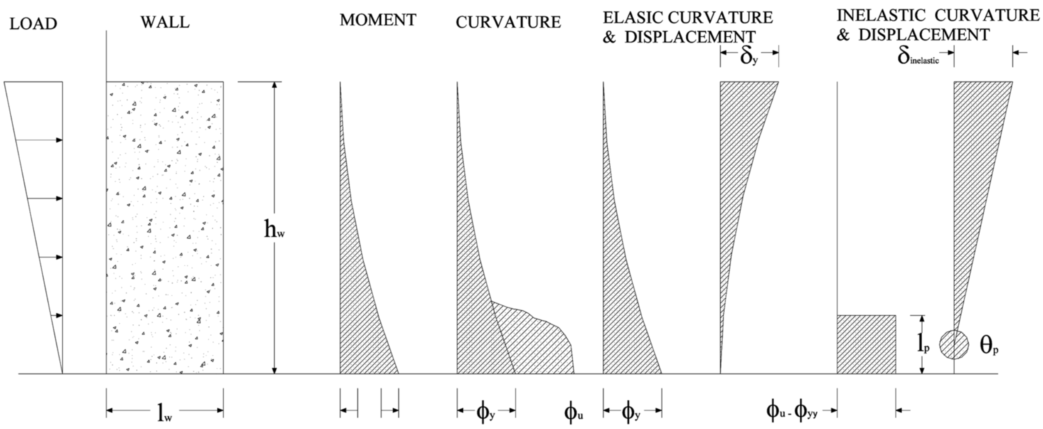

Fig. 16 Wall modeling and deformation components

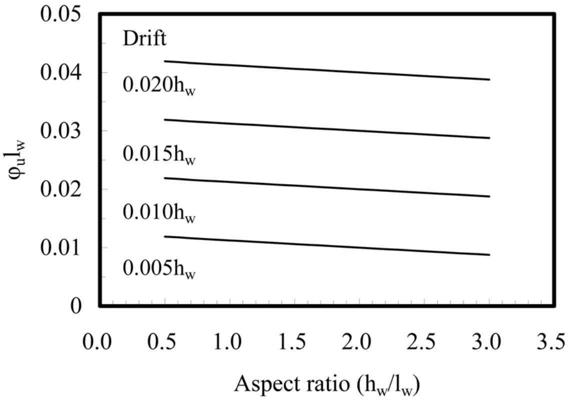

Fig. 17 Required ultimate curvature

required to achieve a given displacement can be solved from (4). The result is expressed in dimensionless form as $\phi_u l_w$ in (5) and plotted in Fig. 17.

$$\phi_u l_w = 0.0025\left(1 - \frac{1}{2}\frac{h_w}{l_w}\right) + 2\frac{\delta_u}{h_w} \tag{5a}$$

To evaluate the test results with respect to the analytical studies presented above sections of this paper requires a modification to (5a) to account for the different in load application (point load at the top of the wall specimen versus a linearly increasing load over the height of the building for a building system). The modified form of (5a) is given as (5b).

$$\phi_u l_w = 0.0025\left(1 - \frac{2}{3}\frac{h_w}{l_w}\right) + 2\frac{\delta_u}{h_w} \tag{5b}$$

The deformation capacity of a wall cross section can be estimated using the model of Fig. 18. The wall has uniformly distributed reinforcement plus boundary steel. The longitudinal tension and compression reinforcement is assumed to develop a stress of αf_y and γf_y, respectively, to account for possible material overstrength and strain hardening ($\alpha = 1.50$ and $\gamma = 1.25$ are used in the subsequent analyses). Based on equilibrium of the wall cross section, the following relations can be derived for framed walls.

$$\varepsilon_{cu} = \left[\frac{\rho\frac{\alpha f_y'}{f_c'} + \rho''\frac{\alpha f_y''}{f_c'} - \rho'\frac{\gamma f_s'}{f_c'} - \frac{\alpha_1 b}{l_w t_w}(a - t_w) + \frac{N}{l_w t_w f_c'}}{\left(\alpha_1\beta_1 + 2\rho''\frac{\alpha f_y''}{f_c'}\right)}\right]\phi_u l_w \tag{6}$$

where ε_{cu} is extreme fiber concrete strain; $\rho = A_s/l_w t_w$ is the tension steel reinforcing ratio; $\rho' = A_s'/l_w t_w$ is the compression steel reinforcing ratio; $\rho'' = A_s''/l_w t_w$ is the distributed steel reinforcing ratio; N is axial load; f_y is nominal yield stress of the web steel; f_s' is stress in the compression steel; t_w is web thickness; b is length of the boundary element; a is thickness of the

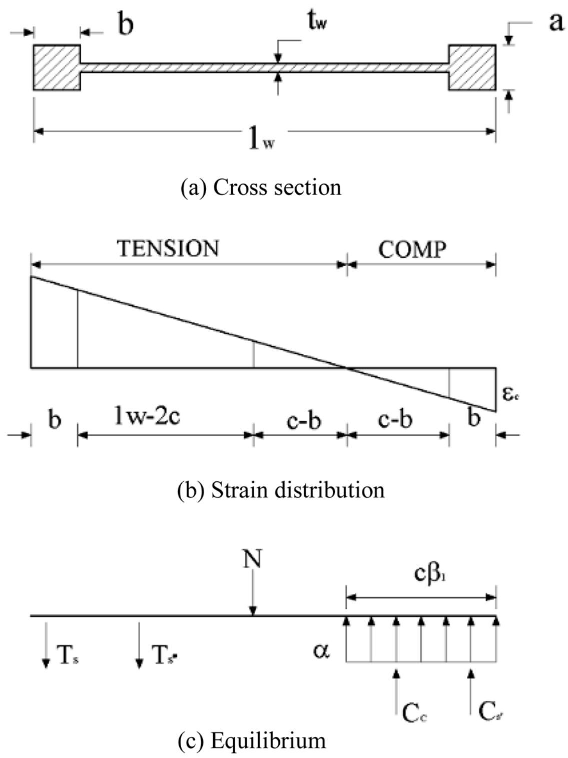

Fig. 18 Equilibrium requirements for barbell-shaped wall cross section

boundary element; and α_1 and β_1 are parameters to define the depth and stress intensity of the equivalent rectangular stress block (shown in Fig. 18) as given by MacGregor (1997):

$$\alpha_1 = 0.85 - \frac{f_c'}{800} \geq 0.725 \tag{7a}$$

$$\beta_1 = 0.95 - \frac{f_c'}{400} \geq 0.700 \tag{7b}$$

The need to provide concrete confinement at the boundary elements of structural walls can be evaluated by substituting (5) into (6). The equations indicate that the maximum concrete compressive strain for a structural wall depends on wall reinforcing ratios, wall axial stress, material properties, and wall aspect ratio.

Fig. 19 plots the computed extreme fiber compression strain for high strength concrete framed shear walls (for $f_y = f_y' = 414$ MPa, $f_y'' = 572$ MPa, $\rho = \rho' = 0.00557$, $\rho'' = 0.00388$), and reveals that extreme fiber compression strain: (1) Increases with the level of axial stress; (2) decreases in wall aspect ratio; and (3) increases with as the roof drift increases. Fig. 19 provides a convenient means of evaluating the need to provide transverse reinforcement for boundary concrete confinement of high strength concrete shear walls.

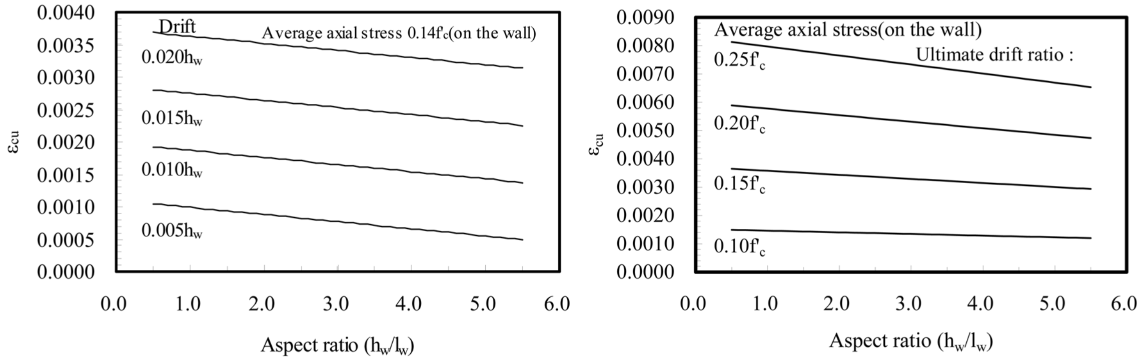

(a) For constant axial stress (b) For constant ultimate drift ratio

Fig. 19 Computed wall extreme fiber strain

The effectiveness of detailing requirements for boundary concrete confinement based on displacement-based design procedure can be assessed by comparing the calculated drift capacity with test results of HSC structural walls with barbell cross section. To calculate the available drift capacity of test specimens using Eq. (5) based on transverse reinforcement details of boundary elements, ultimate extreme fiber concrete strain ε_{cu} must be decided. As shown in Eq. (6), the maximum drift capacity of a HSC wall section may be limited by the ultimate extreme fiber concrete strain including the effect of confinement by the transverse reinforcement. A good measure for the confining action of the transverse reinforcement is $f_{yh}\rho_{sey}$, where f_{hy} is the yield strength of transverse reinforcement; and ρ_{sey} is the effective sectional ratio of confinement reinforcement in y direction.

Most available measurements of ε_{cu} are for columns under axial loads with uniform strain distribution, which is not representative of but similar to the strain distribution in the compressive zone of structural walls. Lėgeron and Paultre (2003) proposed a rational uniaxial stress-strain model to account for confinement of concrete columns with a wide range of concrete strength and transverse reinforcement yield strength. The model was validated on test results from more than 200 circular and HSC square large-scale columns tested under slow and fast concentric loading.

Experimental evidence from concentric compressive tests of tied columns shows that transverse ties do not always reach yield at peak loads, especially when the ties are made of high yield strength steel. However, the confining steel always yields at postpeak strain, ε_{cc50} measured at 50% of the maximum stress on the stress-strain curve. This is due to the large concrete expansion that takes place after the peak. Therefore, the maximum confined concrete strain of framed wall boundary elements, ε_{cu}, is assumed to be equivalent to ε_{cc50}, proposed by Lėgeron and Paultre, given by

$$\varepsilon_{cc50} = \varepsilon_{c50}\left[1 + 60K_e\left(\frac{A_{shy}}{sa}\right)\frac{f_{hy}}{f_c'}\right] = \varepsilon_{cu} \tag{8}$$

where ε_{c50} is corresponding postpesk strain in the unconfined concrete measured at $0.5f_c'$. The strain ε_{c50} is very difficult to measure experimentally. Few experimental values are available in the literature. In the absence of data, it is possible to use $\varepsilon_{c50} = 0.004$ as suggested by Cusson and

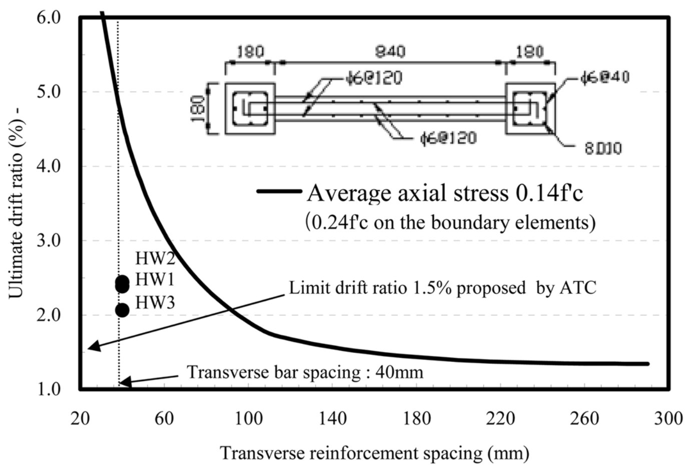

Fig. 20 Comparison of computed and measured ultimate drift ratio

Paultre (1995). It should be noted that for high strength concrete, low values have been reported (Sheikh *et al.* 1994) depending on the type of aggregates and mix proportioning, but in most cases, 0.004 is a reasonable estimate for ε_{c50}. f_{hy} is yield strength of transverse reinforcement; K_e is geometrical effectiveness coefficient of confinement reinforcement introduced by Sheikh and Uzumeri (1982) and by Mander *et al.* (1984); A_{shy} is the area of transverse reinforcement within spacing s.

Bold line in Fig. 20 shows available drift ratio, for HW1 specimen, calculated using the displacement-based design procedure suggested by Wallace with transverse reinforcement spacing. Fig. 20 compares the calculated available drift capacity (HW1 specimen) and the experimentally obtained drift capacity for the tested walls. As can be seen, the computed drift capacity is considerably larger than the value obtained from the experiment as available for HSC framed walls since failure of framed walls was not initiated at the extreme fiber of boundary elements but at the boundary of wall panel and boundary elements (shown in Fig. 6), then strength drop occurred. However, it was considered that the displacement-based design approach is relatively simple to be applied to preliminary design and may provide a valuable tool for evaluating the vulnerability of existing construction.

5. Conclusions

The following conclusions are drawn based on the results of tests of high-strength concrete flexural walls:

1. Testing of high-strength concrete structural walls subjected to high axial stresses, up to $0.24f'_c$, shows that it is possible to ensure a predominantly ductile performance by promoting flexural yielding of the vertical reinforcement. Thus, in this respect, the behavior of high strength concrete is not significantly different from that of normal strength concrete.
2. The axial-load ratio had an important effect on the failure mode, hysteresis loop, stiffness, deformation characteristics and ductility of the high-strength concrete flexural walls. High-

strength concrete flexural walls initially subjected to high level of axial stress, $0.24f'_c$, load showed an 89% enhancement in horizontal load capacity compared with the capacity of wall not subjected to axial load.

3. Higher depths of neutral axis were observed with increasing levels of axial compressive load applied to the wall specimen. HW1 and HW2 specimen, subjected to axial load, failed in a predominantly flexural mode, characterized by the concrete crushing and reinforcement buckling at the lower compressive zone of the boundary elements. The failure region, plastic hinge zone, was more extensive with axial load increasing. Web concrete crushing was observed for HW3 specimen.
4. The predicted strengths from ACI 318-02 Building Code and AIJ Guideline underestimated the measured load-carrying capacities of the high-strength concrete flexural walls tested. ACI and AIJ formulas seem slightly conservative based on the experiment results.
5. Overall moment-curvature response is well correlated with the tested high-strength concrete walls for the confined concrete model proposed by Razvi. Reinforcement stress-strain characteristics were modeled using monotonic relationship that closely resembled the experimentally determined results.
6. The displacement-based design approach is relatively simple to be applied to preliminary design of walls and may provide a valuable tool for evaluating the vulnerability(deformability) of existing walls. But the analytical approach overestimated the measured drift capacity as available for HSC framed walls.

References

ACI Committee 318 (2002), "Building code requirements for structural concrete (ACI318-02) and commentary (ACI318R-02)", American Concrete Institute, Michigan.

Architectural Institute of Japan (AIJ) (1994), "AIJ structural design guidelines for reinforced concrete buildings based on ultimate strength concept", AIJ, Tokyo.

Darwin, D. and Nmai, C.K. (1986), "Energy dissipation in RC beams under cyclic load", *J. Struct. Eng.*, ASCE. **112**(8), 1829-1846.

Ehsani, M.R. and Wright, J.K. (1990), "Confinement steel requirements for connections in ductile frames", *J. Struct. Eng.*, ASCE, **116**(3), 751-767.

Eurocode 8 (1994), "Design provisions for earthquake resistance of structures", ENV 1998.1, Brussels.

Gupta, A.K. and Maestrini, S.R. (1990), "Tension stiffness model for reinforced concrete bars", *J. Struct. Eng.*, ASCE, **116**(3), 769-790.

Gupta, A. and Rangan, B.V. (1998), "HSC structural walls", *ACI Struct. J.*, **95**(2), Mar.-Apr., 194-204.

Kabeyasawa, T. and Hiraishi, H. (1993), "Test and analyses of high-strength reinforced concrete shear walls in Japan", ACI SP 176-13, 281-310.

Lefas, I. (1988), "Behaviour of reinforced concrete structural walls and its implication for ultimate limit state, design", PhD Thesis, University of London.

Légeron, F. and Paultre, P. (2003), "Uniaxial confinement model for normal- and high-strength concrete columns", *J. Struct. Eng.*, ASCE, **129**(2), 241-252.

MacGregor, J.G. *et al.* (1997), "Modification of the ACI rectangular stress block for high-strength concrete", *ACI Struct. J.*, **94**(2), 40-48.

Paulay, T.A. (1986), "Design of ductile reinforced concrete structural walls for earthquake resistance", *Earthquake Spectra*, **2**(4), 783-823.

Paulay, T.A. and Priestley, M.J.N. (1992), *Seismic Design of Reinforced Concrete and Masonry Buildings*, John Wiley & Sons, Inc., 744pp.

Razvi, S. and Saatcioglu, M. (1999), "Confinement model for high-strength concrete", *J. Struct. Eng.*, ASCE, **125**(3), March, 281-289.

Wallace, J.W. (1994), "New methodology for seismic design of RC shear walls", *J. Struct. Eng.*, ASCE, **120**(3), 863-884.

Wallace, J.W. and Moehle, J.P. (1992), "Ductility and detailing requirements of bearing wall buildings", *J. Struct. Eng.*, ASCE, **118**(6), 1625-1644.

Yun, H.D., Choi, C.S. and Lee, L.H. (2004), "Behaviour of high-strength concrete flexural walls", *Proc. of the Inst. of Civil Engineers, Structures and Buildings*, **157**, SB2, 137-148.

Yun, H.D., Choi, C.S. and Lee, L.H. (2004), "Earthquake loading of high-strength concrete walls", *Proc. of the Inst. of Civil Engineers, Structures and Buildings*, **157**, SB3, 201-209.

Zhang, Y.F. and Wang, Z.H. (2000), "Seismic behavior of reinforced concrete shear walls subjected to high axial loading", *ACI Struct. J.*, **97**(5), Sept.-Oct., 739-750.